

## EB2003 SYMPOSIUM | Mitochondrial Nitric Oxide

# Differing roles of mitochondrial nitric oxide synthase in cardiomyocytes and urothelial cells

Anthony Kanai,<sup>1</sup> Michael Epperly,<sup>3</sup> Linda Pearce,<sup>4</sup> Lori Birder,<sup>1</sup> Mark Zeidel,<sup>1</sup> Susan Meyers,<sup>1</sup> Joel Greenberger,<sup>3</sup> William de Groat,<sup>2</sup> Gerard Apodaca,<sup>1</sup> and James Peterson<sup>4</sup>

Departments of <sup>1</sup>Medicine, <sup>2</sup>Pharmacology, and <sup>3</sup>Radiation Oncology, University of Pittsburgh; and Department of <sup>4</sup>Chemistry, Carnegie Mellon University, Pittsburgh, Pennsylvania 15261

Submitted 1 August 2003; accepted in final form 15 August 2003

**Kanai, Anthony, Michael Epperly, Linda Pearce, Lori Birder, Mark Zeidel, Susan Meyers, Joel Greenberger, William de Groat, Gerard Apodaca, and James Peterson.** Differing roles of mitochondrial nitric oxide synthase in cardiomyocytes and urothelial cells. *Am J Physiol Heart Circ Physiol* 286: H13–H21, 2004; 10.1152/ajpheart.00737.2003.—The existence of mitochondrial nitric oxide (NO) synthase (mtNOS) has been controversial since it was first reported in 1995. We have addressed this issue by making direct microsensor measurements of NO production in the mitochondria isolated from mouse hearts. Mitochondrial NO production was stimulated by Ca<sup>2+</sup> and inhibited by blocking electrogenic Ca<sup>2+</sup> uptake or by using NOS antagonists. Cardiac mtNOS was identified as the neuronal isoform by the absence of NO production in the mitochondria of mice lacking the neuronal but not the endothelial or inducible isoforms. In cardiomyocytes from dystrophin-deficient (*mdx*) mice, elevated intracellular Ca<sup>2+</sup>, increased mitochondrial NO production, slower oxidative phosphorylation, and decreased ATP production were detected. Inhibition of mtNOS increased contractility in *mdx* but not in wild-type cardiomyocytes, indicating that mtNOS may protect the cells from overcontracting. mtNOS was also implicated in radiation-induced cell damage. In irradiated rat/mouse urinary bladders, we have evidence that mitochondrially produced NO damages the urothelial “umbrella” cells that line the bladder lumen. This damage disrupts the permeability barrier thereby creating the potential to develop radiation cystitis. RT-PCR and Southern blot analyses indicate that mtNOS is restricted to the umbrella cells, which scanning electron micrographs show are selectively damaged by radiation. Simultaneous microsensor measurements demonstrate that radiation increases NO and peroxynitrite (ONOO<sup>-</sup>) production in these cells, which can be prevented by transfection with manganese superoxide dismutase (MnSOD) or instillation of NOS antagonists during irradiation or irradiation of bladders devoid of mtNOS. These studies demonstrate that mtNOS is in the cardiomyocytes and urothelial cells, that it is derived from the neuronal isoform, and that it can be either protective or detrimental. peroxynitrite microsensors; radiation cystitis

IN THIS PAPER we describe the first functional demonstration of mitochondrial nitric oxide (NO) synthase (mtNOS) in the heart and its identification as the  $\alpha$ -splice variant of neuronal NOS (nNOS $\alpha$ ). We also report on a new demonstration of mtNOS in the epithelial cell lining (urothelium) of the urinary bladder and address the differing roles of mtNOS in these two tissues.

The existence of a NOS localized in the mitochondria was originally described in immunohistochemical studies published

between 1995 (3, 22) and 1996 (4). Because all the known NOS isoforms are encoded by nuclear DNA, and NOS is not encoded by mitochondrial DNA, this finding implied that one of the recognized NOS isoforms was targeted to the mitochondria after protein synthesis in the cytosol. In these early studies, it was reported that the endothelial NOS (eNOS) isoform was localized to the inner mitochondrial membrane in all tissues that were tested, which included the brain, kidney, liver, and skeletal and cardiac muscle. Between 1997 and 1998, more in-depth studies using a variety of NO detection techniques with isolated rat liver mitochondria (14), submitochondrial particles (SMPs), and purified NOS enzyme (17, 18, 37) added further support for the existence of a mtNOS. However, these studies were unable to determine whether the enzyme was novel or related to the neuronal (nNOS), inducible (iNOS), or eNOS isoforms. By 2000, some laboratories (8, 13, 15, 16) had extended their studies to the investigation of the functional implications of mtNOS, whereas others (26) used a NO-sensitive dye to stain the mitochondria in intact cells and to demonstrate the presence of NO within these organelles. Even though this fluorescence technique showed that there is NO within the mitochondria, it could not definitively establish whether the NO reacting with the dye was produced in the mitochondria or whether it was derived from cellular sources. Likewise, in those studies using NOS antibodies to label mtNOS in intact cells, it could be argued that there was cross-reactivity with other proteins or problems with interpretation because of low levels of NOS and high levels of background reactivity. In the studies using isolated mitochondria, SMPs, or purified NOS enzyme, it could similarly be argued that the reported mtNOS was merely one of the cellular isoforms that contaminated the different preparations. Thus, despite a number of positive reports by different laboratories, skepticism remained regarding the existence of a mtNOS. In 2001, our laboratory (19) was the first to use microsensors to electrochemically measure NO production in individual mitochondria isolated from wild-type mouse hearts. Similar measurements from mitochondria isolated from the hearts of iNOS<sup>-/-</sup> and eNOS<sup>-/-</sup>, but not nNOS $\alpha$ <sup>-/-</sup>, mice demonstrated that mtNOS in cardiomyocytes was the nNOS $\alpha$  splice variant. In 2002, a variety of biochemical techniques were used with rat liver mitochondria to demonstrate that mtNOS was the

Address for reprint requests and other correspondence: A. J. Kanai, Renal Electrolyte Division, Univ. of Pittsburgh School of Medicine, A1224 Scaife Hall, Pittsburgh, PA 15261 (E-mail: ajk5@pitt.edu).

The costs of publication of this article were defrayed in part by the payment of page charges. The article must therefore be hereby marked “advertisement” in accordance with 18 U.S.C. Section 1734 solely to indicate this fact.

nNOS $\alpha$  splice variant in this tissue as well and that it contained two posttranslational modifications: acylation with myristic acid and phosphorylation at the COOH terminus (11).

One of the first reported pathological consequences of mtNOS is a putative involvement in the initiation of radiation-induced cell [Chinese hamster ovary (CHO)-K1] damage (23, 24). Whereas ionizing radiation is known to activate a variety of pro- and antiproliferative cytoplasmic transduction pathways (32), the underlying mechanism is unclear (32). Ionizing irradiation produces bursts of superoxide ( $O_2^-$ ) in cells within  $10^{-13}$  s of irradiation exposure. However, it has been calculated that the amounts of  $O_2^-$  and hydrogen peroxide ( $H_2O_2$ ; resulting from  $O_2^-$  dismutation) formed during a clinical radiation dose (1–10 Gy; 1 Gy = 1 J/kg = 100 rad) is less than the amounts generated during normal cellular metabolism (39). One plausible theory is that ionization radiation opens the mitochondrial permeability transition pore, flooding the matrix with  $Ca^{2+}$  that turns on mtNOS. The NO in turn inhibits the respiratory chain resulting in the generation of large amounts of  $O_2^-$ . This  $O_2^-$  then reacts back on the NO to form ONO $^-$  and a cascade of events leading to apoptotic or necrotic cell death. To test this theory, we studied radiation-induced damage (radiation cystitis) in the urinary bladders of rats and mice. Pathologically, radiation cystitis occurs in three distinct phases (34), the earliest of which involves damage to the urothelial cells that line the bladder lumen. To protect the underlying nerves, blood vessels, and bladder smooth muscle from toxic substances in the urine, the large apical or umbrella cells of the urothelium establish an extremely high transepithelial resistance ( $R_t$ ;  $\sim 2,000 \Omega \cdot cm^2$ ) (25), which results in a very low passive permeability to ions and other large molecules. This high-resistance barrier function is due to two factors. First, the protein uroplakin, which is only expressed in the umbrella cells, limits transcellular transport (41, 42). Second, the elaborate tight junctions that connect umbrella cells to one another limit paracellular transport. Thus disruption of this permeability barrier can lead to urine infiltration and cystitis.

## MATERIALS AND METHODS

Purest available grades of all reagents were obtained from Sigma-Aldrich unless otherwise specified. All procedures involving animals were carried out under an approved protocol and in accordance with the guidelines of the Institutional Animal Care and Use Committee of the University of Pittsburgh.

**Isolation of mitochondria and cardiomyocytes.** Tightly coupled mitochondria or cardiomyocytes were isolated from 8- to 12-wk-old wild-type, knockout (nNOS $^{-/-}$ , iNOS $^{-/-}$ , or eNOS $^{-/-}$ ), or *mdx* (dystrophin-deficient) mouse hearts as previously described (10, 19). A suspension of tightly coupled mitochondria or  $Ca^{2+}$ -tolerant cardiomyocytes was gently applied dropwise to collagen-coated dishes and allowed to settle out and attach. The dish with organelles or cells was placed in a temperature-regulated holder mounted on the stage of an inverted microscope (Olympus IX 81). Mitochondrial or cardiomyocyte solution entered the chamber from one end (0.1–1.0 ml/min) and drained out the other. Drugs were either added to the bath along with the perfusate or were locally applied to an organelle or cell by means of a remote-controlled positive displacement nanoejector (Drummond Scientific; Broomall, PA). The nanoejector was mounted on a remote-controlled micromanipulator (1- $\mu m$  resolution) that allows the glass tip of the ejector to be positioned upstream and proximal to an organelle or cell.

**Isolation and culture of urothelial cells.** Urothelial cells were isolated, cultured, and characterized as previously described (6, 38)

with modifications. Bladders were excised from deeply anesthetized (70 mg/kg ip pentobarbital sodium) Sprague-Dawley rats, cut open, and gently stretched and pinned (urothelial surface up) in a Sylgard dish. The tissue was incubated overnight in minimal essential medium (Cellgro, Mediatech; Herndon, VA), penicillin-streptomycin-fungizone, and 2.5 mg/ml dispase (Invitrogen; Rockville, MD). The bladder urothelium was then gently scraped from underlying tissue, treated with 0.25% trypsin, and resuspended in keratinocyte medium (Invitrogen). The dissociated cell suspension (0.1 ml, 50,000–150,000 cells/ml) was plated on the surface of collagen-coated dishes for use as primary cells (basal and transitional cells) within 1–3 days or cultured on the porous support membranes of transwell filter plates for  $\sim 7$ –14 days for the development of a superficial layer of umbrella cells. A positive reaction to cytokeratin was used as proof of the cells epithelial origin. ZO-1 was selected as a marker for tight junctions between epithelial cells, and uroplakin was chosen as a marker for the umbrella cells.

**NO and ONOO $^-$  microsensor preparation and use.** NO and ONOO $^-$  microsensors (tip, 0.1–15  $\mu m$ ; detection, 1–10 nM; response, 1 ms) were prepared from carbon strands (1–5 fibers, 5  $\mu m$  diameter each; BP-AMOCO; Alpharette, GA). Monomeric tetrakis-(3-methoxy-4-hydroxyphenyl)-nickel(II)porphyrin (TMHPPNi; synthesized by us or Frontier Scientific; Logan, UT) was dissolved in 0.1 N NaOH and 2,9,16,23-tetraaminophthalocyanine manganese(II) [MnTAPc; synthesized by us and as previously described (1)] in DMSO. These agents were then deposited, as a polymeric film, on carbon fibers (TMHPPNI or MnTAPc) using cyclic voltammetry ( $-0.2$  to  $+1.0$  V; 20 cycles; 283 EG&G potentiostat; Princeton Applied Research, Oak Ridge, TN). The cation exchanger Nafion (Sigma) was applied to microsensors used for NO measurements by dipping in a 1% ethanolic solution. The negative charges of the  $SO_3^-$  functional group of Nafion keep negatively charged species from gaining access to the catalytic surfaces of NO sensors. Alternatively, the ONOO $^-$  microsensors were coated with the anion exchanger poly(4-vinylpyridine) or PVP (Aldrich) by dipping in a 1% methanolic solution. The positive charges of PVP prevent the diffusion of positively charged species to the catalytic surface of ONOO $^-$  sensors.

The microsensors were characterized by differential pulse voltammetry to determine the redox potentials of NO and ONOO $^-$ . To measure NO or ONOO $^-$ , we used chronoamperometry or differential pulse amperometry. Chronoamperometry for NO was performed at a constant potential 50 mM more positive than its redox potential ( $\sim 0.68$  V). Differential pulse amperometry for ONOO $^-$  was set at 0.2 V for 100 ms, with the applied potential sequentially altered between 0.2 and 0.0 V; the measured current being the difference between the values at these two potentials. High purity ( $>99.99\%$ ) NO and ONOO $^-$  standards were prepared for accurate calibration as previously described (5, 20). The currents generated by the catalytic oxidation of NO and the catalytic reduction of ONOO $^-$  were amplified, converted to voltages, and digitized for real-time viewing on a monitor or storage on hard disk for later retrieval and analysis.

In vitro microsensor measurements of NO production in isolated mitochondria and cardiomyocytes were accomplished as previously described (19). The simultaneous measurement of NO and ONOO $^-$  from bladder sheets was accomplished as follows. Isolated sheets were pinned in a temperature-regulated (37°C) bath, and the preparation was continuously perfused with Ringer solution (containing in mM: 144 Na $^+$ , 5.4 K $^+$ , 1 Mg $^{2+}$ , 1.8 Ca $^{2+}$ , 10 glucose, and 10 phosphate; pH 7.4). Solution entered the chamber from one end (0.1–1.0 ml/min) and drained out the other. The microsensors were mounted on separate ultramicromanipulators, and, with the aid of a microscope, their tips were positioned adjacent to one another on the surface of a tissue strip. Drugs were either added to the bath or were locally applied to the tissue via a remote-controlled positive displacement nanoejector (Drummond Scientific; Broomall, PA). The tip of the ejector was positioned upstream and proximal to the microsensors.

*Video-detected cardiomyocyte shortening as a measure of contractility.* The percent shortening of electrically stimulated cardiomyocytes was used as a determinant of myocardial force generation. Signals were recorded by using a video edge motion detector (VED105; Crescent Electronics, Sandy UT) and charge-coupled device camera system (FTM800; Philips Electronics). A given cell was viewed on a monitor, and two raster points were locked on either end of the long axis of the cell. The temporal resolution of the system is 4.2 ms.

*Irradiation of the urinary bladder.* Sprague-Dawley rats or nNOS<sup>-/-</sup>, iNOS<sup>-/-</sup>, eNOS<sup>-/-</sup>, and C57BL10 control mice were anesthetized (1–3 mg/kg im ketamine) and irradiated with 1 or more fractions of radiation (0–50 Gray) with intervals of 1–3 days between fractions. The irradiation was delivered by a 6 MV Varian Clinac 6/100 linear accelerator (Varian Medical Instruments; Palo Alto, CA), with the beam reduced to 15 × 15 mm (rats) or 10 × 10 mm (mice) so that only the area encompassing the bladder was exposed. To further minimize the risk of damage to the hematopoietic system and bowels, the animals were placed supine, in Trendelenburg's position, so that the pelvis was elevated thereby allowing the intestines to shift forward and away from the radiation beam.

*MnSOD plasmid-liposome complex delivery.* The plasmid-liposome complexes were prepared by mixing 75 μl of lipofectin liposomes with 1.33 mg of plasmid DNA in a volume of 133 μl of PBS and incubated for 30 min at room temperature. At this point, 592 μl of water were added to the complexes, and the mixture was stored at 4°C while the rats ( $n = 4-6$ ) were prepared for bladder catheterization. In preparation, each rat was first weighed and then anesthetized with inhalation of halothane (5% induction, 2.5% maintenance). When the pedal reflex was absent, the bladder of each rat was catheterized with a 3-Fr Tom Cat catheter (NLS Animal Health; Baltimore, MD). Bladders were then irrigated with 0.5 ml of water, which was allowed to drain. This rinsing decreased any possible damage to the plasmid-liposome complex due to the osmotic effects of the urine. Then 600 μl of the plasmid-liposome complex (containing 500 μg of plasmid DNA) were instilled into each bladder lumen and held there for 15 min. The delivered dose was 600 μl because there is a 200-μl dead space in the catheter. After 15 min, the catheters were removed and the rats were allowed to recover. Control rats were injected with either saline or plasmid-liposome complex without plasmid DNA.

*Diffusive permeability measurements.* The transepithelial resistance and [<sup>3</sup>H]water and [<sup>14</sup>C]urea permeabilities were measured using a specially designed Ussing chamber as previously described by our laboratory (21).

## RESULTS AND DISCUSSION

*Identification of mtNOS in isolated cardiac mitochondria.* Mitochondrial purity was assessed as the ratio of mitochondrial protein, determined spectrophotometrically as cytochrome *c* oxidase content, to total protein (10). This varied from ~40 to 90% in the particular case of mitochondria from wild-type cells, whereas the variation in NO production by individual mitochondria was  $28 \pm 9$  nM ( $n = 8$ , four different preparations), arguing very strongly against the measured activity being caused by nonmitochondrial contaminants. In addition, direct electrode measurements performed on the supernatant from the last step of the mitochondrial purification procedure showed an absence of NOS activity. Nevertheless, all mitochondrial preparations are, to some extent, contaminated with other organelles. Isolation procedures based on Percoll gradients, either as a single step (29) or in addition to differential centrifugation (36), still contain 10% or more other materials. The use of heart tissue leads to mitochondrial preparations that are less contaminated with microsomal fractions than if liver

was the starting tissue. Moreover, pelleting of mitochondria at ~10,000 *g* (rather than the ~100,000 *g* used in many published procedures) ensures that significantly smaller microsomes essentially remain dispersed throughout the supernatant. Because mouse cardiomyocytes are ~37.5% mitochondria as a percentage of cell volume and only ~1% sarcoplasmic reticulum (33), heart preparations exhibit a higher ratio of mitochondria to contaminating organelles than preparations starting from other tissues. In the mouse skeletal muscle, for example, the mitochondria comprise only ~2% of the cell volume. The key feature of our approach is that we measure NO production from individual mitochondria to overcome the problem of background contamination. The mitochondria, which always swell during isolation, are 2 to 3 μm in diameter and are resolvable under phase optics. In contrast, microsomes are <0.5 μm in diameter and are not detectable. In all of our active preparations, 80–90% of the individual mitochondria tested (6–12 per each of 14 preparations) produced NO. None of the individual mitochondria in preparations that were uncoupled either by aging or application of protonophores produced NO. The notion that the remarkably reproducible production of NO by only coupled mitochondria could be due to low levels of contaminants that would have to be similarly associated with 80–90% of the individual mitochondria tested appears extremely improbable. The additional observation that the results are quantitatively invariant between active preparations further argues against the measured effects being caused by contaminants.

Withdrawing the microsensor tip (in 1-μm increments) from a mitochondrion generating NO enabled us to determine that mitochondrially produced NO diffused  $\leq 10$  μm in our experimental setup ( $8 \pm 2$  μm;  $n = 24$ ). Thus, by sparsely plating to provide a >10-μm zone around the mitochondrion from which we were recording, we were assured that the NO signals detected were derived from a single mitochondrion. Initially, with a microsensor positioned next to a mitochondrion, there was no detectable basal NO production. However, the addition of Ca<sup>2+</sup> (10 μM) by itself evoked sustained NO production (Fig. 1, A and B). Supplementation of the mitochondria with L-arginine (1 mM) or tetrahydrobiopterin (10 μM) did not increase NO formation. This result implies that the mitochondria contain all of the substrate and cofactors necessary for NOS activity except for Ca<sup>2+</sup>. The fact that this NO production is inhibitable by the NOS antagonists N<sup>G</sup>-monomethyl-L-arginine (L-NMMA, 100 μM; Fig. 1B) or 7-nitroindazole (7-NI, 50 μM; not shown) demonstrates that it is being produced by a NOS. Moreover, the finding that this NO production is inhibited by blocking Ca<sup>2+</sup> uptake through the electrogenic uniporter with ruthenium red (1 μM; Fig. 1C) or by collapsing the membrane potential with a protonophore [carbonyl cyanide *p*-trifluoromethoxyphenylhydrazone (FCCP), 100 nM; or carbonyl cyanide *m*-chlorophenylhydrazone (CCCP), 100 nM; not shown] demonstrates that the measured NO is coming from mtNOS and not a cellular NOS contaminating the preparation.

The Ca<sup>2+</sup>-evoked production of NO could be blocked with the nonselective NOS antagonist L-NMMA (100 μM; Fig. 1B). However, the blockade of NO production could be achieved with a lower dose of the nNOS-selective antagonist 7-NI (50 μM; not shown), suggesting that mtNOS may be related to the nNOS isoform. This similarity of mtNOS to the neuronal isoform was confirmed by the absence of NO production in

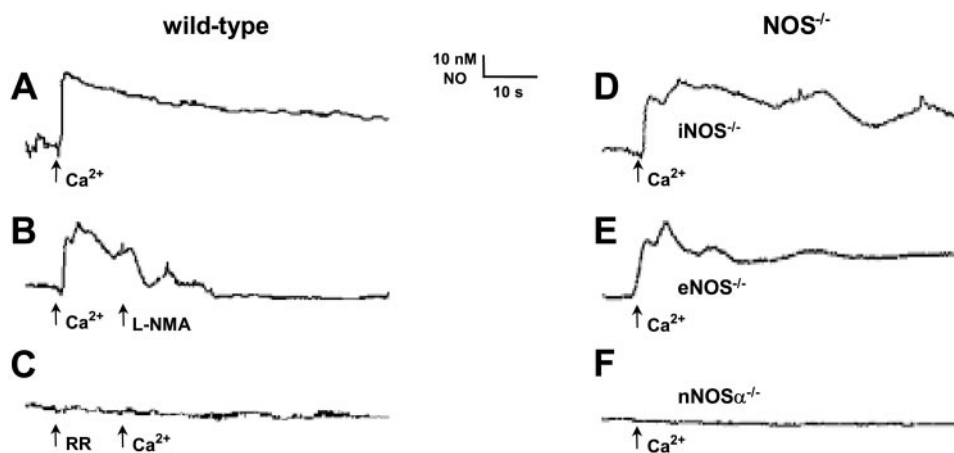


Fig. 1. A–F: electrochemical demonstration of nitric oxide (NO) production and the identification of the neuronal NO synthase (nNOS) isoform in isolated cardiac mitochondria. A porphyrinic microsensors were used to measure NO production by individual tightly coupled cardiac mitochondria. Organelles were in aerobic  $\text{Ca}^{2+}$ -free mitochondrial solution without supplemental L-arginine or cofactors, under which conditions there was no detectable NO production. When exogenous  $\text{Ca}^{2+}$  ( $10 \mu\text{M}$ ) was added to the bath, it evoked a rapid production of NO ( $28 \pm 9 \text{ nM}$ ;  $n = 8$ , A and B), which was inhibited by the addition of the NOS antagonists *N*<sup>G</sup>-monomethyl-L-arginine (L-NMMA,  $100 \mu\text{M}$ ; B) or 7-nitroindazole ( $50 \mu\text{M}$ ; not shown).  $\text{Ca}^{2+}$ -dependent production of NO was also inhibited by pretreatment with ruthenium red (RR,  $1 \mu\text{M}$ ; C), a blocker of the electrogenic uniporter that is responsible for  $\text{Ca}^{2+}$  uptake by mitochondria. Identification of nNOS $\alpha$  as the isoform of cardiac mitochondrial NOS (mtNOS) was deduced by using mitochondria isolated from the hearts of knockout mice for the inducible (iNOS $^{-/-}$ ; D), endothelial (eNOS $^{-/-}$ ; E), and neuronal (nNOS $\alpha^{-/-}$ ; F) isoforms. Only mitochondria isolated from the hearts of nNOS $\alpha^{-/-}$  mice failed to produce NO ( $n = 5$ ).

mitochondria isolated from the hearts of knockout mice for the neuronal but not the endothelial or inducible NOS isoforms (Fig. 1, D and E). There are at least three nNOS alternative-splice variants: nNOS $\alpha$ , nNOS $\beta$ , and nNOS $\gamma$  (28, 30). Only the nNOS $\alpha$  variant is knocked out in the nNOS $^{-/-}$  mouse, which is accomplished by deleting exon-2 near the NH<sub>2</sub> terminus. This exon contains the postsynaptic disks-large zoe-1 (PDZ) motif responsible for tethering nNOS to membranes (7, 9, 35). Both the eNOS $^{-/-}$  and iNOS $^{-/-}$  mice have their respective NOS gene entirely knocked out, neither of which has been shown to contain a PDZ motif. Because mtNOS is reported to be membrane bound (3, 4, 22), it may be tethered through this PDZ-binding domain. Alternatively, mtNOS may be tethered through a posttranslational modification involving acylation with myristic acid as recently reported (11).

**Protective role of mtNOS in *mdx* cardiomyocytes.** To determine the effects of mitochondrially produced NO on bioenergetics, we used intact cardiomyocytes from *mdx* mice. Norepinephrine (NE)-evoked NO production by caveolar-associated eNOS (Fig. 2A) is abolished (Fig. 2C) or greatly decreased (by ~83%, not shown) in *mdx* cardiomyocytes. However, a new beat-to-beat production of NO, which we propose is coming from mtNOS, is readily observed in *mdx* cells in response to electrical stimulation (Fig. 2D). Although we cannot unequivocally state that beat-to-beat NO production is entirely absent in the case of the wild-type cardiomyocytes, it is certainly at or below our detection limit ( $1 \text{ nM NO}$ ; Fig. 2B). We further hypothesize that the observed increase in mtNOS activity represents an attempt by the *mdx* cell to compensate for the low eNOS activity in caveolae. Thus, by using only those cardiomyocytes that fail to respond to NE, we are afforded the opportunity to study mtNOS in intact cells in the absence of the cytosolically produced NO.

Although contractility (video-detected shortening) is decreased by about 50% in *mdx* cardiomyocytes compared with wild-type cells, inhibition ( $100 \mu\text{M}$  L-NMMA) of beat-to-beat

NO production recovered about half of this lost contractility (Fig. 2F). On the other hand, the inhibition of NO production in wild-type cardiomyocytes had no observable effects on contractility (Fig. 2F). Abolition of beat-to-beat NO production by collapsing the mitochondrial membrane potential with a protonophore uncoupler (FCCP,  $100 \text{ nM}$ ; Fig. 2E) further supports our hypothesis that this NO production is of mitochondrial origin. These observations also suggest that prolonged elevation of cellular  $\text{Ca}^{2+}$ , a hallmark of dystrophin-deficient cells, activates mtNOS resulting in local NO production that can transiently inhibit mitochondrial ATP production and, in turn, contractility. In *mdx* cells, where the absence of dystrophin results in a weakening of the sarcolemmal membrane, this decrease in contractility may be a protective mechanism to guard against myocardial damage.

Although the muscular dystrophies are most readily recognized for their skeletal muscle involvement, Duchenne muscular dystrophy (DMD) patients also have a cardiomyopathy. In Becker muscular dystrophy, which is allelic to DMD, the cardiomyopathy may be severe and may be the principle manifestation of dystrophin deficiency. Because the absence of dystrophin from the sarcolemma may weaken the skeletal and cardiac muscle membrane alike, making them leaky to  $\text{Ca}^{2+}$  and more susceptible to stretch-induced damage, it is interesting to speculate that the role of mitochondrially produced NO in the pathological myocardium may be to limit myocardial contractility and thus protect the heart. Inhibition of ATP production and contractility would, however, subsequently lead to cardiac hypertrophy and eventually heart failure as observed in patients with both Duchenne and Becker muscular dystrophies. Because mtNOS is present in wild-type cardiomyocytes, it may serve a similar role under physiological conditions (in which mitochondrially produced NO could protect the healthy myocardium from over work by limiting ATP production during acute  $\text{Ca}^{2+}$  overload) that may accompany strenuous exercise or other stressors.

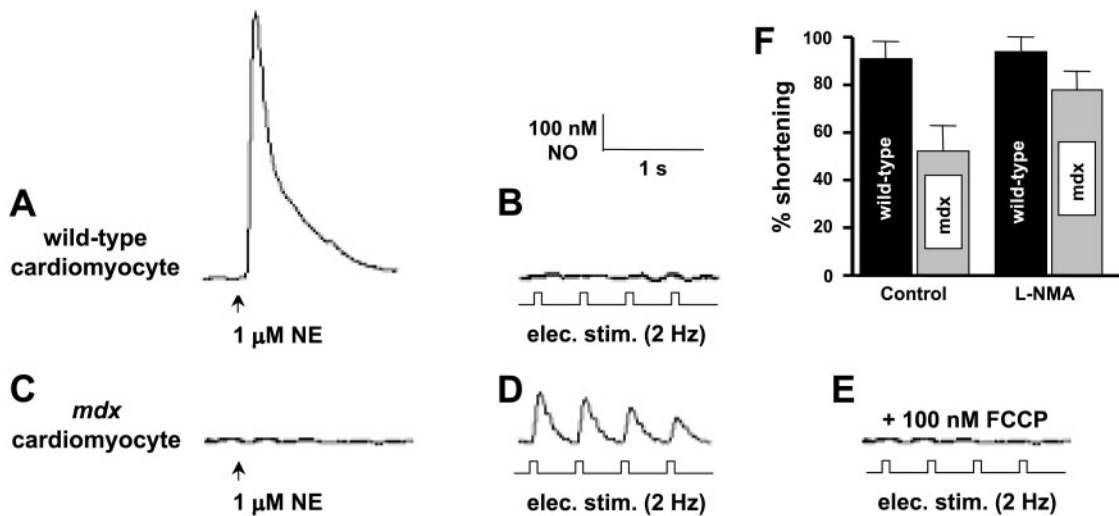


Fig. 2. A–F: inhibition of beat-to-beat NO production in dystrophin-deficient (*mdx*) cardiomyocytes increases contractility. Norepinephrine (NE; 1  $\mu$ M) evoked NO ( $726 \pm 260$  nM;  $n = 7$ ) production in a quiescent wild-type cardiomyocyte (A), whereas pacing (voltage =  $2 \times$  threshold; duration = 10 ms; frequency = 2 Hz) the cell did not evoke detectable NO formation (B). In dystrophin-deficient (*mdx*) cardiomyocytes, however, NE (1  $\mu$ M) evoked a diminished NO response ( $126 \pm 90$  nM;  $n = 7$ ; not shown) or none at all ( $n = 5$ ; C), whereas pacing the cells released NO ( $141 \pm 94$  nM;  $n = 12$ ; D) beat to beat. Blockade of electrically stimulated NO production in *mdx* cells was accomplished by inhibiting the electrogenic  $Ca^{2+}$  uniporter. This was rapidly and reversibly accomplished by collapsing the membrane potential with the protonophore uncouplers carbonyl cyanide *p*-trifluoromethoxyphenylhydrazone (FCCP, 100 nM;  $n = 5$ ; E) or carbonyl cyanide *m*-chlorophenylhydrazone (CCCP, 100 nM;  $n = 4$ ; not shown). Administration of NOS antagonists L-NMMA (100  $\mu$ M;  $n = 7$ ; not shown) or 7-nitroindazole (50  $\mu$ M;  $n = 6$ ; not shown) also effectively inhibited electrically stimulated beat-to-beat NO production in *mdx* cardiomyocytes. Although contractility in *mdx* cardiomyocytes was approximately half that of normal cells, inhibition of NO production with L-NMMA (or 7-nitroindazole) increased contractility by approximately one-fourth in *mdx* cells ( $n = 7$ ) but had no effect on normal cells ( $n = 8$ ; F).

Identification of *mtNOS* in umbrella cells of the bladder urothelium. The luminal surface of the urinary bladder consists of a multilayered epithelium composed of apical, transitional, and basal cells, which establish an effective permeability

barrier to ions and other molecules in the urine. The large apical or umbrella cells (Fig. 3B) of the urothelium establish an extremely high  $R_t$  ( $\sim 2,000 \Omega \cdot \text{cm}^2$ ) (25). The relevant resistances are shown in the electrical equivalent circuit (Fig.

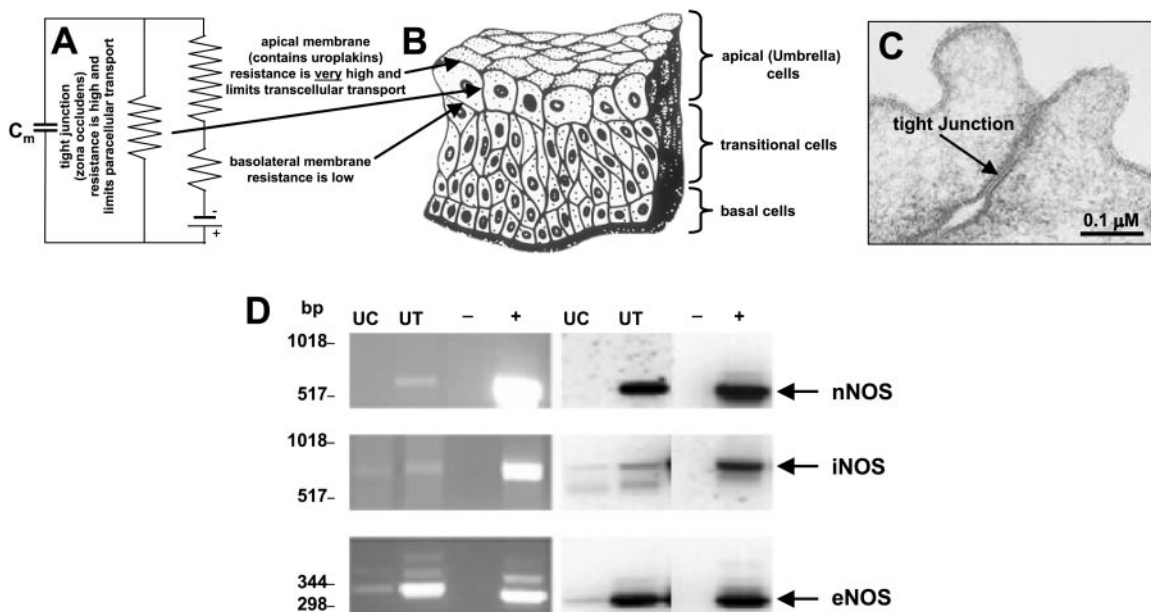


Fig. 3. A–C: electrical equivalent circuit for a urinary bladder umbrella cell (A); a drawing of the urothelium depicting the basal, transitional, and apical (umbrella) cell layers (B); and an electron micrograph of two adjacent umbrella cells in rabbit urothelium showing a tight junction (C, arrowhead). D: ethidium bromide-stained agarose gels of the RT-PCR products (left) and Southern blots (right) of bladder urothelial tissue (UT) and cultured urothelial cells (UC). UT contains urothelial cells, along with connective, vascular, and nervous tissue. –, No template control; +, rat brain cDNA as a template. Expected product size: eNOS, 343 bp; iNOS, 827 bp; and nNOS, 701 bp. For nNOS, the positive and negative control lanes for the Southern blot are from a shorter exposure to prevent masking of fainter signals.

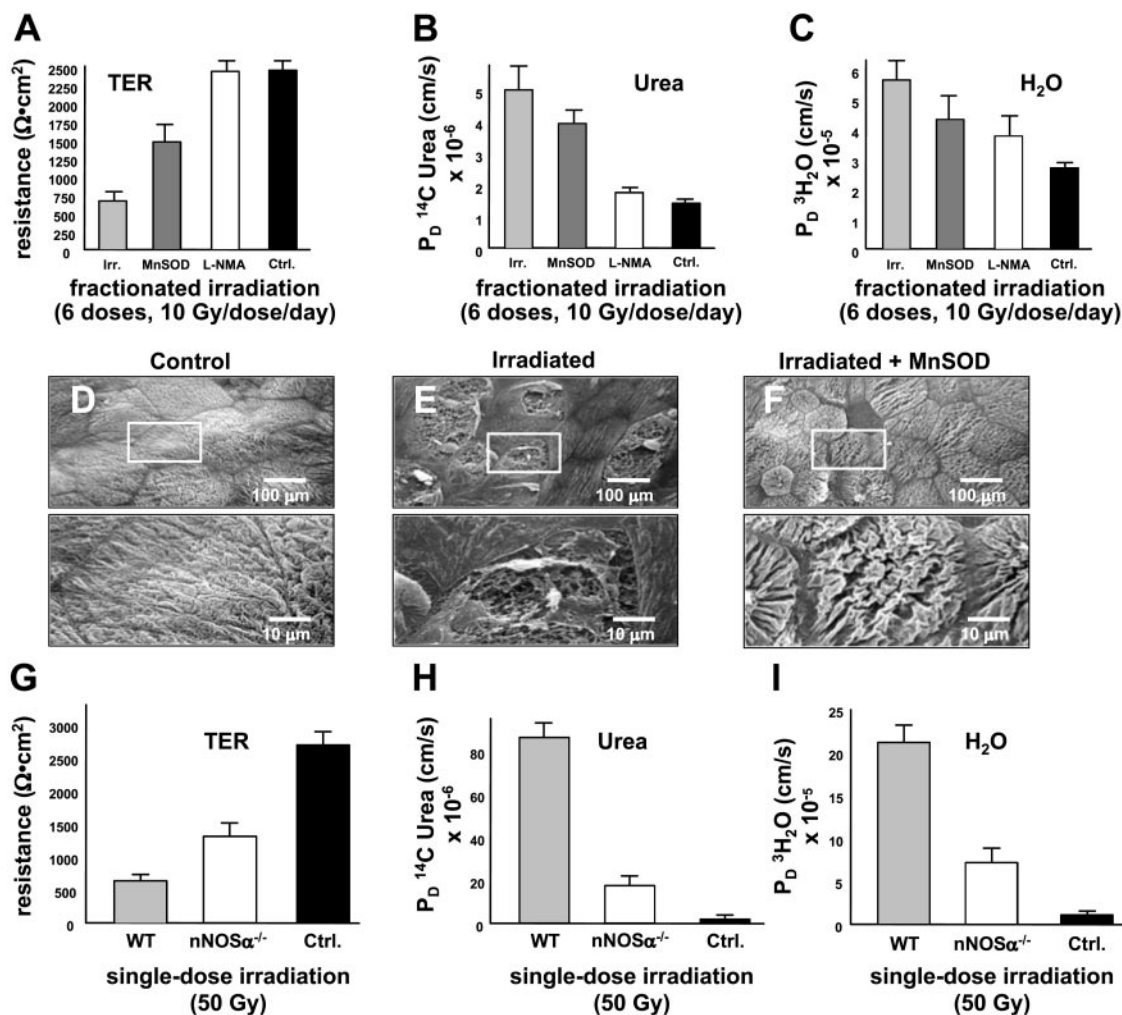


Fig. 4. A–C: results of a fractionated-radiation (6 doses, 10 Gy $\cdot$ dose $^{-1}$  $\cdot$ day $^{-1}$ ; 1 Gy = 1 J/Kg = 100 rads) study comparing nonirradiated bladders (Ctrl;  $n = 12$ ) with irradiated bladders (Irr;  $n = 8$ ), bladders transfected with the human MnSOD transgene before each radiation dose (MnSOD;  $n = 6$ ), and bladders instilled with a NOS antagonist (L-NMMA, 500  $\mu\text{M}$ ;  $n = 6$ ) during each radiation dose. The use of the NOS antagonist was more effective than MnSOD treatment and prevented radiation-induced changes in transepithelial resistance (TER, A) and urea permeability (B) and was more protective in preventing increases in water permeability (C). D and E: scanning electron micrographs depicting changes that occurred in the urothelium after fractionated-irradiation. Bottom: magnified areas enclosed by the rectangles in the top micrographs. D: nonirradiated bladder shows normal intact urothelium ( $n = 7$ ); E: after irradiation the bladders show areas of superficial ulceration of the umbrella cells ( $n = 6$ ); F: bladder urothelium transfected with the human MnSOD transgene before irradiation shows only minimal ulceration. G–I: results of a single high-dose (50 Gy) radiation study. In nonirradiated mouse bladders (Ctrl), the intact permeability barrier exhibits high TER (G) and low urea (H) and water (I) permeabilities. At 24 h after irradiation (wild-type, WT), resistance is decreased and permeabilities are increased ( $n = 4$ ). However, in knockout mice devoid of nNOS $\alpha$  (nNOS $\alpha^{-/-}$ ), the damaging effects of irradiation on permeabilities are markedly decreased ( $n = 4$ ).

3A). The total resistance is the sum of the apical (very high), junctional (high), and basolateral (low) resistances. The very high apical resistance is due to the protein uroplakin, which is only expressed in umbrella cells and only in the apical membrane and its underlying vesicles, (41, 42). The high-junctional resistance is due to the elaborate tight junctions that connect the umbrella cells to one another (Fig. 3C, arrowhead).

Whereas adequate numbers of organelles could be isolated from mouse hearts to make measurements from isolated mitochondria feasible, given the mass of the heart and the high mitochondrial content of cardiomyocytes [ $\sim 30\%$  of cell volume (2)], this was not possible with the urothelial umbrella cells, which constitute only a single cell layer. Therefore, it

was necessary to use an alternate approach to determine whether there is mtNOS in the umbrella cells and if it is the neuronal isoform.

We used ethidium bromide-stained agarose gels of RT-PCR products (Fig. 3D, left) and Southern blots (Fig. 3D, right) to determine the presence or absence of NOS isoforms in the primary cultures of urothelial cells and urothelial tissue. Urothelial tissue consists of urothelial cells along with small amounts of connective, vascular, and nervous tissue, whereas primary cultures consist mainly of transitional and basal cells because the umbrella cells do not survive the isolation process. This is evident by the lack of uroplakin in these cells (not shown). To develop striated layers, including terminally differentiated umbrella cells, primary cells must be cultured on

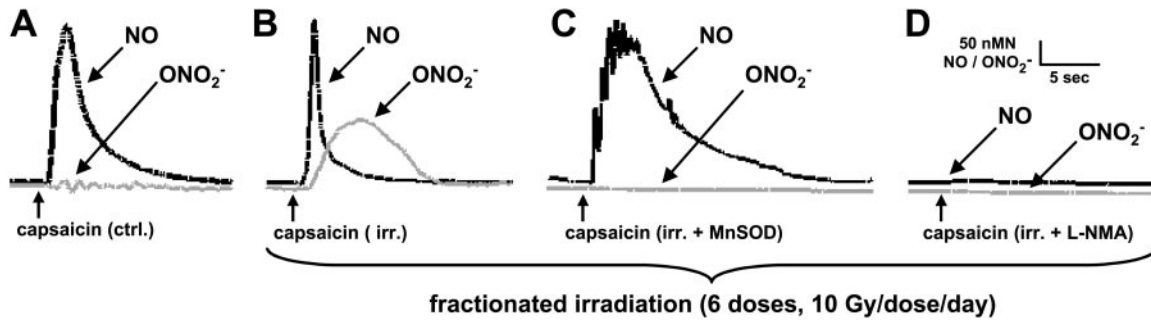


Fig. 5. Simultaneous in vitro microsensor measurements of NO and peroxynitrite ( $\text{ONOO}^-$ ) production in the mouse bladder urothelium in response to the administration of capsaicin ( $1 \mu\text{M}$ ). Bladders were excised, cut open, and pinned flat with the urothelium facing up in a temperature-regulated ( $37^\circ\text{C}$ ) bath. Tips of the microsensors were positioned adjacent to one another, directly on the surface of the urothelium. A: nonirradiated control (Ctrl); B: after fractional irradiation (6 doses,  $10 \text{ Gy}\cdot\text{dose}^{-1}\cdot\text{day}^{-1}$ ) of a nontreated mouse bladder; C: after fractional irradiation of a bladder transfected with the human transgene for MnSOD 12 h before each radiation dose; D: after fractional irradiation of a bladder with L-NMMA ( $100 \mu\text{M}$ ) present in the bladder lumen during each radiation dose.

the porous membranes of transwell filter plates for  $\sim 7$  to 14 days.

Figure 3D demonstrates that nNOS, eNOS, and iNOS (trace amounts) are present in urothelial tissue preparations (transitional cells and umbrella cells) and that in cell preparations containing only basal and transitional cells without umbrella cells, nNOS is lost. This suggests that the primary location for nNOS is the umbrella cells. These results are supported by direct microsensor measurements from the surface of bladder strips, where the agonist (capsaicin;  $500 \text{ nM}$ ) evoked NO production (by nNOS) was reversibly blocked by collapsing the mitochondrial membrane potential ( $\Delta\psi$ ) with the protonophore uncoupler FCCP ( $10\text{--}100 \text{ nM}$ ) or CCCP ( $10\text{--}100 \text{ nM}$ ) (not shown). Alternately, in isolated primary cells, agonist-evoked (NE,  $1 \mu\text{M}$ ) NO production (by eNOS) was not inhibited by FCCP or CCCP (not shown).

**Deleterious role of mtNOS in urothelial cells.** A large number of patients in the United States undergo irradiation for pelvic malignancies each year. However, the total allowable radiation dose is limited by the potential for developing radiation-induced cystitis (31). Acute damage following irradiation consists of urothelial swelling, ulceration, and vascular endothelial cell damage. A subacute phase follows within 4–6 days with infiltration of inflammatory cells (27). A third chronic phase is associated with collagen deposition and fibrosis,

leading to decreased bladder compliance (27). Importantly, the available pathological evidence indicates that urothelial damage is prominent in the early phase following radiation exposure.

In the clinical setting, radiation is typically given in fractionated doses spread over a number of days. Accordingly, we conducted fractionated dose experiments and utilized a group of animals of which their bladders were transfected with the human MnSOD transgene before irradiation as well as a group of animals of which their bladders were instilled with the NOS antagonist L-NMMA ( $500 \mu\text{M}$ ) during irradiation. In Fig. 4, A–C, it is apparent that NOS antagonism was more effective than MnSOD treatment and prevented radiation-induced changes in  $R_t$  (Fig. 4A) and urea permeability (Fig. 4B) and was more protective in preventing increases in water permeability (Fig. 4C).

The scanning electron microscopy was used to examine the ultrastructure of urothelial cells and to evaluate the changes that occur following irradiation. The areas enclosed by the rectangles in the upper micrographs are shown magnified in the lower micrographs. In control (nonirradiated) bladders, the urothelium was intact (Fig. 4D). In irradiated bladders, however, there are areas of superficial ulceration of umbrella cells (Fig. 4E). It is important to note that whereas all the cells of the urothelium are exposed to the ionizing radiation beam, the

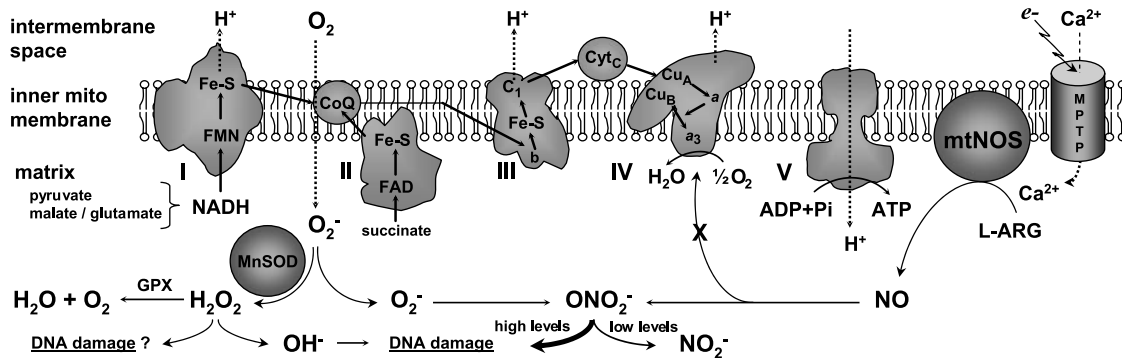


Fig. 6. Scheme depicting inner mitochondrial membrane and the five subunits of the mitochondrial electron transport chain: I, NADH dehydrogenase; II, succinate dehydrogenase; III, cytochrome c reductase; IV, cytochrome c oxidase; V, ATP synthase; CoQ, coenzyme Q; and cyt c, cytochrome c. Also included in the scheme are the putative locations of MnSOD, mitochondrial permeability transition pore (MPTP), and mitochondrial NO synthase (mtNOS).

damage appears to be restricted to the umbrella cells. Transfection with the human MnSOD transgene, on the other hand, helped to protect the urothelium as it only showed minimal ulceration (Fig. 4F). To visualize the transfection efficiency of the plasmid-liposome complexes used in these experiments at the tissue level, a construct containing the LacZ transgene in place of MnSOD was instilled into bladders. LacZ-transfected bladders show that positive staining was restricted to the umbrella cell layer ( $n = 4$ ; not shown). Further support for the involvement of mtNOS in radiation cystitis is presented in the study depicted in Fig. 4, G–I. In this figure, it is demonstrated that the absence of nNOS (nNOS $\alpha^{-/-}$ ) has a protective effect on  $R_t$  (Fig. 5G) and urea (Fig. 5H) and water (Fig. 5I) permeabilities in mice receiving a large (50 Gy) single dose of irradiation.

We used direct microsensor measurements from the umbrella cell layer of the bladder to determine the effects of ionizing radiation on the levels of NO and ONOO $^-$ . In nonirradiated (control) bladders, capsaicin-evoked NO production resulted in negligible ONOO $^-$  formation (Fig. 5A), whereas in irradiated bladders it resulted in significant ONOO $^-$  formation (Fig. 5B). Alternatively, both MnSOD overexpression (Fig. 5C) and inhibition of NOS with L-NMMA (Fig. 5D) suppressed ONOO $^-$  formation. These first simultaneous microsensor measurements of NO and ONOO $^-$  demonstrate that ONOO $^-$  formation is significant when levels of NO and O $_2^-$  are elevated and that this consequence can be ameliorated by superoxide dismutase (MnSOD) and/or a NOS inhibitor (L-NMMA).

We hypothesize that ionization-radiation opens the mitochondrial permeability transition pore, flooding the matrix with Ca $^{2+}$ , and thus activating mtNOS (Fig. 6). The elevated NO, in turn, inhibits cytochrome oxidase (complex IV) in the respiratory chain increasing O $_2^-$  formation at coenzyme Q. Accordingly, the presence of high levels of MnSOD may be therapeutic and dismutate the additional O $_2^-$  that is formed. However, in the scheme in Fig. 6, we show that one of the by-products of O $_2^-$  dismutation is H $_2$ O $_2$ , which itself may be toxic to tissues. Furthermore, if glutathione peroxidase (which converts H $_2$ O $_2$  to H $_2$ O and molecular O $_2$ ) levels are insufficient, the toxic hydroxyl radical (OH $^-$ ) may be formed, resulting in tissue damage. Thus, there are potential side effects of MnSOD treatment, but overall the effects are beneficial as demonstrated in Fig. 4, A–C. Several findings from our group support this theory: 1) transfection of cells with SOD was only protective against radiation-induced damage when targeted to the mitochondria (40); and 2) inhibition of NOS during irradiation prevented cellular damage (Fig. 4, A–C). The O $_2^-$  free radical is normally generated within the mitochondria as the toxic by-product of oxidative phosphorylation. However, these levels can dramatically increase when the respiratory chain is inhibited (12).

In conclusion, the above studies demonstrate that mtNOS is in cardiomyocytes and urothelial cells, that it is derived from the neuronal isoform in both cases, and that it may be protective in *mdx* cardiomyocytes but detrimental in irradiated urothelial umbrella cells. The identification of cardiac mtNOS was demonstrated directly by measurements of NO production from isolated mitochondria and the absence of this production in nNOS knockout mice. On the other hand, the isolation of mitochondria from the urothelial umbrella cells is impractical

due to the limited tissue and was demonstrated indirectly by a combination of methods. This distribution of mtNOS in two very diverse tissue types raises the possibility that mitochondrial NO production may be important in many different cell types.

#### GRANTS

This research was supported by National Institutes of Health Grants HL-57985 (to A. Kanai), HL-60132 (to J. Greenberger), HL-61411 (to J. Peterson), and DK-54824 (to L. Birder); American Cancer Society Grant RSG-03-007 (to A. Kanai); and a grant from the Muscular Dystrophy Association (to A. Kanai).

#### REFERENCES

- Achar BN, Fohlen GM, Parker JA, and Keshavayya J. Synthesis and structural studies of metal(II) 4,9,16,23,-Phthalocyanine tetraamines. *Polyhedron* 6: 1463–1467, 1987.
- Barth E, Stammer G, Speiser B, and Schaper J. Ultrastructural quantitation of mitochondria and myofilaments in cardiac muscle from 10 different animal species including man. *J Mol Cell Cardiol* 24: 669–681, 1992.
- Bates TE, Loesch A, Burnstock G, and Clark JB. Immunocytochemical evidence for a mitochondrially located nitric oxide synthase in brain and liver. *Biochem Biophys Res Commun* 213: 896–900, 1995.
- Bates TE, Loesch A, Burnstock G, and Clark JB. Mitochondrial nitric oxide synthase: a ubiquitous regulator of oxidative phosphorylation? *Biochem Biophys Res Commun* 218: 40–44, 1996.
- Beckman JS, Chen J, Ischiropoulos H, and Crow JP. Oxidative chemistry of peroxynitrite. *Methods Enzymol* 233: 229–240, 1994.
- Birder LA, Nealen ML, Kiss S, de Groat WC, Caterina MJ, Wang E, Apodaca G, and Kanai AJ.  $\beta$ -Adrenoceptor agonists stimulate endothelial nitric oxide synthase in rat urinary bladder urothelial cells. *J Neurosci* 22: 8063–8070, 2002.
- Brennan JE, Chao DS, Gee SH, McGee AW, Craven SE, Santillano DR, Wu Z, Huang F, Xia H, Peters MF, Froehner SC, and Bredt DS. Interaction of nitric oxide synthase with the postsynaptic density protein PSD-95 and alpha1-syntrophin mediated by PDZ domains. *Cell* 84: 757–767, 1996.
- Bringold U, Ghafourifar P, and Richter C. Peroxynitrite formed by mitochondrial NO synthase promotes mitochondrial Ca $^{2+}$  release. *Free Radic Biol Med* 29: 343–348, 2000.
- Craven SE and Bredt DS. PDZ proteins organize synaptic signaling pathways. *Cell* 93: 495–498, 1998.
- Darley-Usmar V, Rickwood D, and Wilson MT. *Mitochondria: A Practical Approach*. Oxford: IRL, 1987, p. 1–16.
- Elfering SL, Sarkela TM, and Giulivi C. Biochemistry of mitochondrial nitric-oxide synthase. *J Biol Chem* 277: 38079–38086, 2002.
- Fridovich I. Superoxide radical and superoxide dismutases. *Annu Rev Biochem* 64: 97–112, 1995.
- Ghafourifar P, Klein SD, Schucht O, Schenk U, Pruschy M, Rocha S, and Richter C. Ceramide induces cytochrome c release from isolated mitochondria. Importance of mitochondrial redox state. *J Biol Chem* 274: 6080–6084, 1999.
- Ghafourifar P and Richter C. Nitric oxide synthase activity in mitochondria. *FEBS Lett* 418: 291–296, 1997.
- Ghafourifar P and Richter C. Mitochondrial nitric oxide synthase regulates mitochondrial matrix pH. *Biol Chem* 380: 1025–1028, 1999.
- Ghafourifar P, Schenk U, Klein SD, and Richter C. Mitochondrial nitric-oxide synthase stimulation causes cytochrome c release from isolated mitochondria. Evidence for intramitochondrial peroxynitrite formation. *J Biol Chem* 274: 31185–31188, 1999.
- Giulivi C. Functional implications of nitric oxide produced by mitochondria in mitochondrial metabolism. *Biochem J* 332: 673–679, 1998.
- Giulivi C, Poderoso JJ, and Boveris A. Production of nitric oxide by mitochondria. *J Biol Chem* 273: 11038–11043, 1998.
- Kanai AJ, Pearce LL, Clemens PR, Birder LA, VanBibber MM, Choi SY, de Groat WC, and Peterson J. Identification of a neuronal nitric oxide synthase in isolated cardiac mitochondria using electrochemical detection. *Proc Natl Acad Sci USA* 98: 14126–14131, 2001.
- Kanai AJ, Strauss HC, Truskey GA, Crews AL, Grunfeld S, and Malinski T. Shear stress induces ATP-independent transient nitric oxide

- release from vascular endothelial cells, measured directly with a porphyrinic microsensor. *Circ Res* 77: 284–293, 1995.
21. **Kanai AJ, Zeidel ML, Lavelle JP, Greenberger JS, Birder LA, de Groat WC, Apodaca G, Meyers SA, Ramage R, and Epperly MW.** Manganese superoxide dismutase gene therapy protects against irradiation-induced cystitis. *Am J Physiol Renal Physiol* 283: F1304–F1312, 2002.
  22. **Kobzik L, Stringer B, Balligand JL, Reid MB, and Stamler JS.** Endothelial type nitric oxide synthase in skeletal muscle fibers: mitochondrial relationships. *Biochem Biophys Res Commun* 211: 375–381, 1995.
  23. **Leach JK, Black SM, Schmidt-Ullrich RK, and Mikkelsen RB.** Activation of constitutive nitric-oxide synthase activity is an early signaling event induced by ionizing radiation. *J Biol Chem* 277: 15400–15406, 2002.
  24. **Leach JK, Van Tuyle G, Lin PS, Schmidt-Ullrich R, and Mikkelsen RB.** Ionizing radiation-induced, mitochondria-dependent generation of reactive oxygen/nitrogen. *Cancer Res* 61: 3894–3901, 2001.
  25. **Lewis SA.** Everything you wanted to know about the bladder epithelium but were afraid to ask. *Am J Physiol Renal Physiol* 278: F867–F874, 2000.
  26. **Lopez-Figueroa MO, Caamano C, Morano MI, Ronn LC, Akil H, and Watson SJ.** Direct evidence of nitric oxide presence within mitochondria. *Biochem Biophys Res Commun* 272: 129–133, 2000.
  27. **McDonald S, Rubin P, Phillips TL, and Marks LB.** Injury to the lung from cancer therapy: clinical syndromes, measurable endpoints, and potential scoring systems. *Int J Radiat Oncol Biol Phys* 31: 1187–1203, 1995.
  28. **Putzke J, Seidel B, Huang PL, and Wolf G.** Differential expression of alternatively spliced isoforms of neuronal nitric oxide synthase (nNOS) and N-methyl-D-aspartate receptors (NMDAR) in knockout mice deficient in nNOS alpha (nNOS alpha(delta/delta) mice). *Brain Res Mol* 85: 13–23, 2000.
  29. **Reinhart PH, Taylor WM, and Bygrave FL.** A procedure for the rapid preparation of mitochondria from rat liver. *Biochem J* 204: 731–735, 1982.
  30. **Saur D, Paehge H, Schusdziarra V, and Allescher HD.** Distinct expression of splice variants of neuronal nitric oxide synthase in the human gastrointestinal tract. *Gastroenterology* 118: 849–858, 2000.
  31. **Schellhammer PF, Jordan GH, and el Mahdi AM.** Pelvic complications after interstitial and external beam irradiation of urologic and gynecologic malignancy. *World J Surg* 10: 259–268, 1986.
  32. **Schmidt-Ullrich RK, Dent P, Grant S, Mikkelsen RB, and Valerie K.** Signal transduction and cellular radiation responses. *Radiat Res* 153: 245–257, 2000.
  33. **Sommer JR and Johnson EA.** Ultrastructure of cardiac muscle. In: *Handbook of Physiology. The Cardiovascular System. The Heart.* Bethesda, MD: Am. Physiol. Soc., 1979, sect. 2, vol. I, chapt. 5, p. 113–186.
  34. **Stewart FA, Lundbeck F, Oussoren Y, and Luts A.** Acute and late radiation damage in mouse bladder: a comparison of urination frequency and cystometry. *Int J Radiat Oncol Biol Phys* 21: 1211–1219, 1991.
  35. **Stricker NL, Christopherson KS, Yi BA, Schatz PJ, Raab RW, Dawes G, Bassett DE Jr, Bredt DS and Li M.** PDZ domain of neuronal nitric oxide synthase recognizes novel C-terminal peptide sequences. *Nat Biotechnol* 15: 336–342, 1997.
  36. **Susin SA, Larochette N, Geuskens M, and Kroemer G.** Purification of mitochondria for apoptosis assays. *Methods Enzymol* 322: 205–208, 2000.
  37. **Tatoyan A and Giulivi C.** Purification and characterization of a nitric-oxide synthase from rat liver mitochondria. *J Biol Chem* 273: 11044–11048, 1998.
  38. **Truschel ST, Ruiz WG, Shulman T, Pilewski J, Sun TT, Zeidel ML, and Apodaca G.** Primary uroepithelial cultures. A model system to analyze umbrella cell barrier function. *J Biol Chem* 274: 15020–15029, 1999.
  39. **Ward JF.** DNA damage as the cause of ionizing radiation-induced gene activation. *Radiat Res* 138: S85–S88, 1994.
  40. **Wong GH, Elwell JH, Oberley LW, and Goeddel DV.** Manganous superoxide dismutase is essential for cellular resistance to cytotoxicity of tumor necrosis factor. *Cell* 58: 923–931, 1989.
  41. **Wu XR, Lin JH, Walz T, Haner M, Yu J, Aebi U, and Sun Mammalian uroplakins TT.** A group of highly conserved urothelial differentiation-related membrane proteins. *J Biol Chem* 269: 13716–13724, 1994.
  42. **Yu J, Manabe M, Wu XR, Xu C, Surya B, and Sun TT.** Uroplakin I: a 27-kD protein associated with the asymmetric unit membrane of mammalian urothelium. *J Cell Biol* 111: 1207–1216, 1990.